



Article

# Clevis-Grip Tensile Tests on Basalt, Carbon and Steel FRCM Systems Realized with Customized Cement-Based Matrices

Dario De Domenico <sup>1,\*</sup> , Natale Maugeri <sup>1</sup>, Paolo Longo <sup>1</sup>, Giuseppe Ricciardi <sup>1</sup>, Giuseppe Gulli <sup>2</sup> and Luigi Calabrese <sup>1</sup>

<sup>1</sup> Department of Engineering, University of Messina, Villaggio S. Agata, 98166 Messina, Italy

<sup>2</sup> Tradimalt S.p.A., Via Nazionale 1, 98049 Messina, Italy

\* Correspondence: dario.dedomenico@unime.it; Tel.: +39-0906765921

**Abstract:** The tensile properties of fabric-reinforced cementitious matrix (FRCM) composites are experimentally investigated through clevis-grip tensile tests (according to AC434 provisions) on FRCM coupons realized with customized (ad hoc developed in this paper) cement-based matrices. The tested FRCM coupons are reinforced with basalt, carbon, or steel fabrics, and are prepared with three different matrices: one-component mortar incorporating dispersible copolymer powders of vinyl acetate and ethylene (matrices A and B) and two-component mortar with carboxylated styrene–butadiene copolymer liquid resin (matrix C). This has made it possible to investigate the mechanical compatibility between different mortar matrices and fabrics and the resulting tensile properties of FRCM composites in the uncracked, cracking, and fully cracked phases. Experimental results are critically analyzed in terms of stress–strain curves and failure mechanisms comparatively for the analyzed FRCM systems. It has been shown that the matrix B exhibits a good compatibility with the basalt pre-impregnated fabric, while the matrix C appears to be the most suitable candidate to optimize the interfacial stress transfer at the fiber–matrix interface for all fabrics, thus exalting the mechanical performances in terms of tensile strength and ultimate strain. The results of this experimental program can be useful for designing optimized mortar mixes aimed at realizing novel FRCM composites or at improving existing FRCM systems by suitably accounting for compatibility behavior and slippage at the fabric–matrix interface.

**Keywords:** fabric-reinforced cementitious matrix (FRCM); FRCM coupon; clevis-grip tensile tests; cement-based matrix; customized mortar; basalt fabric; carbon fabric; steel fabric



**Citation:** De Domenico, D.; Maugeri, N.; Longo, P.; Ricciardi, G.; Gulli, G.; Calabrese, L. Clevis-Grip Tensile Tests on Basalt, Carbon and Steel FRCM Systems Realized with Customized Cement-Based Matrices. *J. Compos. Sci.* **2022**, *6*, 275. <https://doi.org/10.3390/jcs6090275>

Academic Editor: Francesco Tornabene

Received: 22 August 2022

Accepted: 15 September 2022

Published: 17 September 2022

**Publisher's Note:** MDPI stays neutral with regard to jurisdictional claims in published maps and institutional affiliations.



**Copyright:** © 2022 by the authors. Licensee MDPI, Basel, Switzerland. This article is an open access article distributed under the terms and conditions of the Creative Commons Attribution (CC BY) license (<https://creativecommons.org/licenses/by/4.0/>).

## 1. Introduction

Fabric-reinforced cementitious matrix (FRCM) systems are being used frequently for retrofitting existing concrete and masonry structures [1,2] as an alternative to the well-known fiber-reinforced polymer (FRP) composites [3,4]. FRCM systems are realized by embedding fibers (in the form of a dry or pre-impregnated fabric having unidirectional or bidirectional configuration) within an inorganic (cement-based, lime-based, or geopolymer mortar) matrix that usually incorporates short polymer fibers [5]. Externally bonded FRCM systems have been used for various structural purposes, such as confinement of reinforced concrete columns [6,7], flexural strengthening [8–10] or shear strengthening [11–13] of reinforced concrete members. Since in all such applications FRCM composites are externally bonded to the concrete/masonry substrate, the effectiveness of this retrofitting technology strongly relies on two factors: (1) the bond behavior at the FRCM–substrate interface and (2) the tensile properties of the composite in the uncracked, cracking, and fully cracked phase involving the fabric–matrix interaction. These properties are inherently related to the matrix–fiber and matrix–substrate compatibility features, as well as to the ability of the matrix to interfacially interact with the fiber yarns. As an example, a common drawback of FRCM systems could be the limited bond adhesion between matrix and

dry fibers, which may give rise to telescopic failure of the fabric [14–16]. It is, therefore, essential to mechanically characterize, through appropriate laboratory tests, these two factors (bond behavior and tensile properties) underlying the mechanical behavior of the FRCM composite as a whole. The former (bond behavior) is generally investigated through single-lap/double-lap shear tests [17–19] or indirect beam tests [20,21]. The latter (tensile properties) can be analyzed through tensile tests on FRCM prismatic coupons [22–26], which provide useful information on tensile strength and axial stiffness of the composite.

There are generally two methods for the mechanical characterization of tensile properties of FRCM coupons, illustrated in Figure 1: (1) the *clamping-grip tensile test*, in which the matrix is directly gripped by four steel plates (or tabs) transferring the tensile load from the testing machine, which induces a shear stress combined with normal stress on the specimen in the gripping zone—this loading configuration is adopted in the Italian guideline CNR-DT 215 [27]—and (2) the *clevis-grip tensile test*, in which the tensile load from the testing machine is transferred to the FRCM coupon through an auxiliary steel tab connected to the steel tabs through a clevis pin, thus producing shear stress without transversal stress in the gripping zone—this loading configuration is adopted in the US guidelines AC434 [28] and ACI 549 [1]. The main feature of clamping-grip tests (and the main difference with respect to clevis-grip tests) is that the gripping pressure should be sufficient to avoid local matrix failure, prevent matrix–textile slippage, and lead to eventual textile rupture.

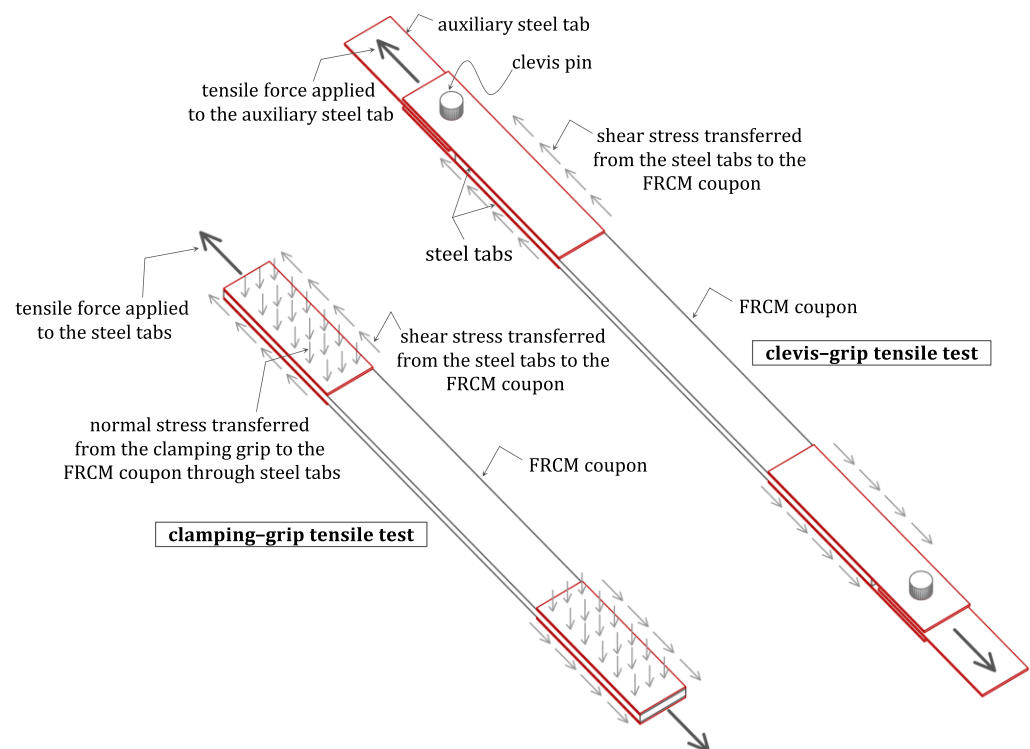


**Figure 1.** Tensile tests on FRCM coupons through clamping-grip (Italian guidelines CNR-DT 215/2018 [27]) and clevis-grip (US guidelines AC434 [28] and ACI 549 [1]) loading configurations.

It is worth noting that the tensile behavior of the FRCM coupons is affected by the bond properties at the fabric–matrix interface because the load is transferred from the matrix to the fabric in both (clevis-grip and clamping-grip) testing configurations through interfacial shear stress [29], although the two testing schemes produce different boundary conditions.

In this paper, the experimental results of clevis-grip tensile tests on FRCM coupons realized with different fibers and customized matrices are presented. In the authors’ opinion, this testing configuration can offer more reliable results because of the absence

of transversal stress along the clamping length, which may exalt micro-defects that occur during the specimen preparation. Moreover, as said above, the results of the clamping-grip tests may be affected by the gripping pressure. The novel contributions of this work compared to other experimental campaigns are here summarized:

- The tensile tests are carried out with the same fabric layout and comparing three different customized (rather than commercial, as typically adopted in papers available from the pertinent literature) cement-based matrices, ad hoc developed in this paper. This has made it possible to evaluate the best compatibility at the fabric–matrix interface for different compositions of mortar.
- The tensile tests are comparatively carried out with the same matrix but different fiber types (basalt, carbon, and steel), thus highlighting the influence of the axial rigidity of the fiber mesh on the mechanical behavior (tensile strength and failure mechanism) of the composite coupon and slippage at the fabric–matrix interface.
- Elastic moduli and stress and strain indicators are computed for all the investigated coupons according to AC434 provisions in order to draw useful conclusions on the mechanical performance of the investigated FRCM systems.

## 2. Materials and Methods

### 2.1. Materials

Three fabrics, consisting of open meshes of fibers having different natures, were used for the preparation of the FRCM coupons: (1) basalt bidirectional (balanced) pre-impregnated fabrics, (2) carbon bidirectional (balanced) dry fiber rovings, and (3) unidirectional steel fabric made of ultra-high strength steel (UHTSS) galvanized wires twisted in cords. This research work belongs to a wider experimental campaign investigating the performance of such kinds of fabrics, quite popular in the field of structural retrofitting of masonry or concrete structures. The photographs of the utilized fabrics along with some detailed microscope images of the joints and of the cross-sections of the single yarns (steel wires) are shown in Figure 2, while their main physical and mechanical properties are listed in Table 1. For high-magnification images, a 3D optical microscope was used (KH-8700 digital microscope, Hirox, Tokyo, Japan).

**Table 1.** Physical and mechanical properties of the fabrics used in the FRCM coupons.

Fabric	Mesh Configuration	Density [g/m <sup>2</sup> ]	Equivalent Thickness $t_f$ [mm <sup>2</sup> /mm]	Elastic Modulus [GPa]	Tensile Strength [MPa]	Ultimate Strain [%]
basalt	balanced	450	0.075	90/75 <sup>†</sup>	3200/1450 <sup>†</sup>	>3/>2.3 <sup>†</sup>
carbon	balanced	220	0.061	240/209 <sup>†</sup>	4700/1850 <sup>†</sup>	>1.8/0.9 <sup>†</sup>
steel	unidirectional	2200	0.27	190	>2200	>1.2

<sup>†</sup> First and second number refers to the filament and to the fabric (per direction) property, respectively.

The three types of fabrics were combined with customized cementitious matrices to constitute the FRCM system. All customized mortar mixes contained ordinary Portland cement (CEM I 52,5 R), aggregates (max grain size 600  $\mu$ m), cellulose-based additives (to improve workability and water-retention properties), resin, short polymer fibers and water. Short polymer (polyacrylonitrile) fibers (nominal diameter 16  $\mu$ m, length 8 mm, specific weight 1.18 g/m<sup>3</sup>, elastic modulus 13.5 GPa) were dispersed in the cementitious paste to prevent plastic shrinkage while improving the curing process. Three different resins/binders were used in the mix design (approximately 2.5% in weight), either in powder (resins A and B) or liquid (resin C) form, whose physical properties are listed in Table 2. The three resins gave rise to three related matrices, called matrix A and B (both one-component matrices) and matrix C (two-component matrix), respectively.

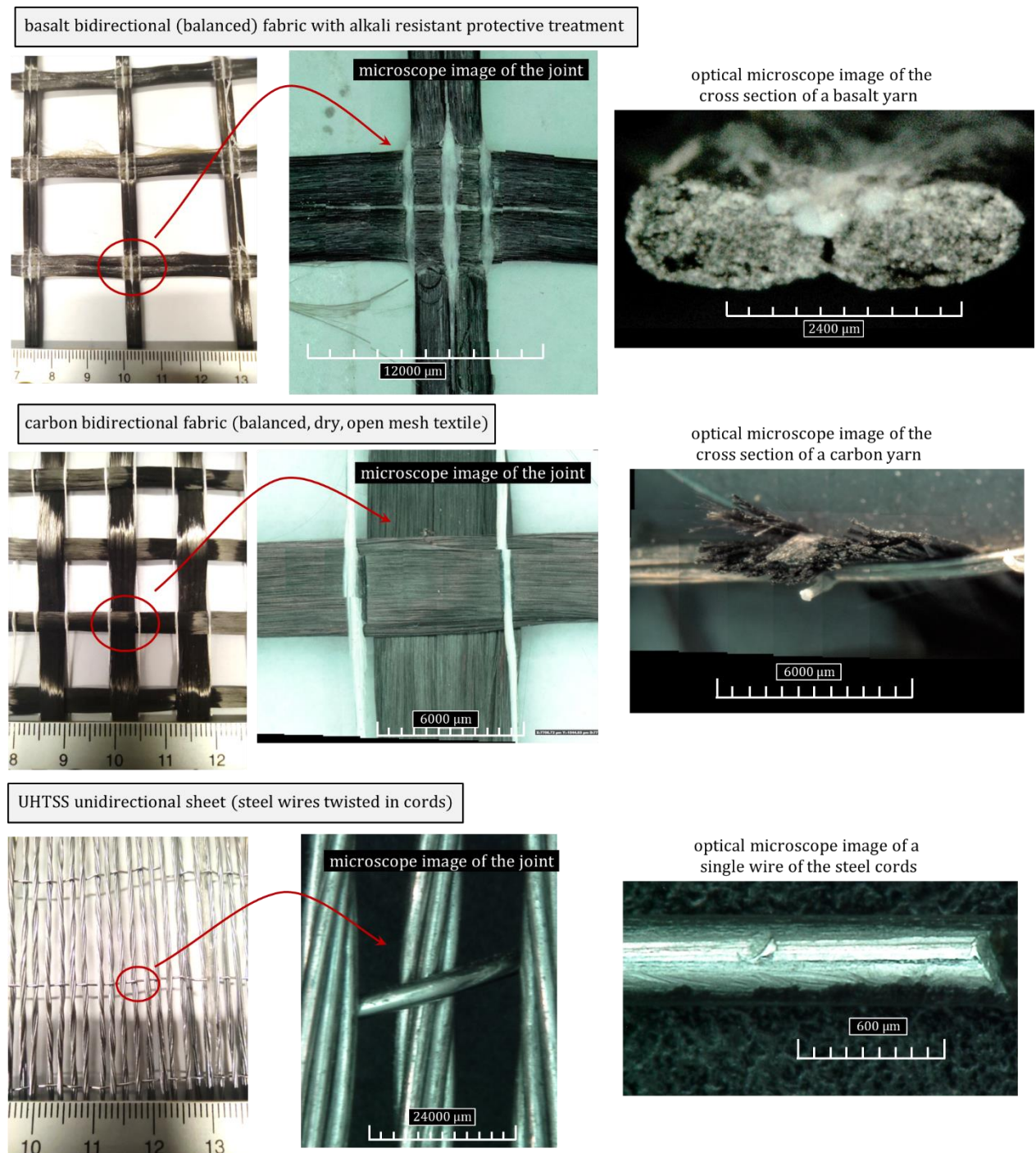


**Figure 2.** Fibers used for preparing FRCM coupons (numbers indicated in rulers on the left-side photos are units in [cm]).

**Table 2.** Physical characteristics of the resins/binders used in the customized cementitious matrices.

Resin	Appearance	Chemical Components	Bulk Density [g/L]
A	free-flowing white powder	copolymer of vinyl acetate, vinyl versatate and ethylene	400–600
B	white to light beige powder	copolymer of vinyl acetate and ethylene	405–555
C	white liquid	carboxylated styrene-butadiene copolymer.	-

In this experimental campaign, each matrix was comparatively used for the three types of fabrics: this made it possible to identify the most suitable resin/binder for improving the adhesion between the cementitious matrix and the fabric. In particular, resin A was a re-dispersible binder based on copolymer of vinyl acetate, vinyl versatate and ethylene, while the resin B, also dispersible in water, was based on copolymer powder of vinyl acetate and ethylene. Although both resins A and B had polyvinyl alcohol as a protective colloid and a similar chemical composition, resin B was softer and more flexible than resin A because of the relatively high ethylene content. Moreover, resin A was associated with a lower ash content (10.5%) than that of resin B (13%), as obtained by thermogravimetric analysis at 1000 °C. On the other hand, resin C was a water-based (aqueous) dispersion of a carboxylated styrene–butadiene copolymer used for modification of hydraulic binders, with a viscosity (Brookfield LVE, 60 rpm) equal to 90 mPa·s as per ISO 1652 standards.

The various ingredients of the cementitious paste were mixed through a pan mixer by adding water gradually until the cement slurry appears of good consistency, in compliance with UNI EN 196-1 specifications. The mix design of the three resulting mortar matrices is reported in Table 3. The lower water content in the matrix C was due to the fact that the water-based resin C inherently contains a small amount of water.

**Table 3.** Mix design (quantities in [kg/m<sup>3</sup>] units) of the cement mortars.

Material	Matrix A & B <sup>†</sup>	Matrix C
Portland cement	460	460
aggregates	1255	1310
additives	2	2
resin	55 <sup>†</sup>	220
polyacrylonitrile fibers	15	15
water	319	110

<sup>†</sup> The mix design of matrix A and B only differs for the type (same proportions) of resin employed.

## 2.2. Mechanical Characterization of Mortar Mixes

The three customized matrices considered in the preparation of the FRCM coupons were mechanically characterized in terms of flexural and compression strength in accordance with UNI EN 196-1 standards. Three prismatic specimens of each mortar (dimensions 40 mm × 40 mm × 160 mm) were poured in metal molds, de-molded after 48 h and left cured at controlled temperature (22 ± 0.5 °C) and humidity conditions (60%). The measured (average) densities of each mortar were 1651 kg/m<sup>3</sup>, 1667 kg/m<sup>3</sup> 1583 kg/m<sup>3</sup> for matrix A, B, and C, respectively. The prismatic specimens of matrices A and C were then tested at 3, 7, and 28 days from casting (those of matrix B are only tested at 28 days) to investigate the evolution of the mechanical properties at different stages of the hardening process.

To determine the flexural strength, three-point bending tests were performed (three specimens for each batch) in load-controlled mode (monotonically increasing load) with a test frame having a load capacity 15 kN (load rate 50 N/s). Then, compression tests were carried out on the two halves of the broken prism with another test frame having 250 kN load capacity (load rate 2400 N/s) by distributing the applied load through two platens of 4 cm side. Test results (average values with error bars) are illustrated in Figure 3. In general, the two-component matrix C exhibited a lower performance than the one-component matrix A in the early curing times (3 days) but considerably better mechanical behavior during the development of the hardening process (+20% and +30% at 7 and 28 days in terms of flexural strength, +33% at 28 days in terms of compression strength). Matrix B (only tested at 28 days) exhibited the worst performance among the three considered matrices, with strength results slightly lower than those pertinent to matrix A. The quite narrow error bars reveal low dispersion in the obtained experimental findings.

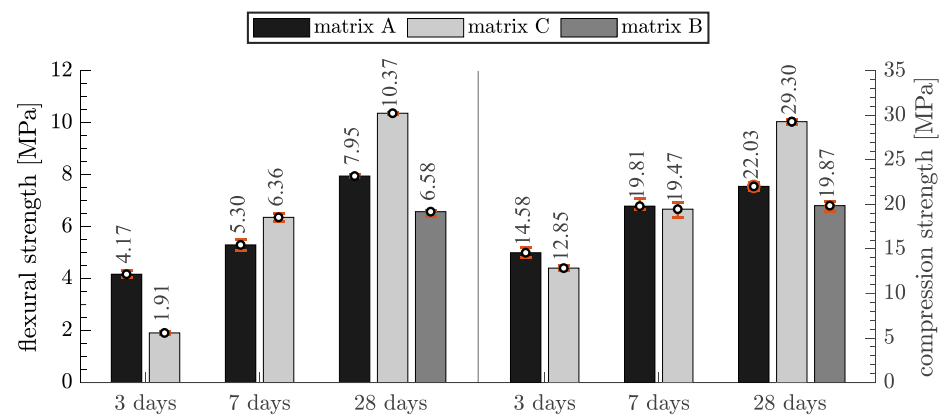


Figure 3. Flexural and compression strength of mortar matrices according to UNI EN 196-1.

It is worth noting that the matrices developed in this work exhibit a relatively higher flexural strength and compression strength than alternative, commercial cement-based matrices adopted in other literature papers, e.g., [30,31].

### 2.3. Preparation of FRCM Coupons for Tensile Tests

The three matrices were used for fabricating prismatic coupons having nominal dimensions of 50 mm × 600 mm × 10 mm (width × length × thickness). These dimensions are based on the Italian guidelines for the tensile qualification of FRCM systems [32]—Annex 1.

Differently from other literature studies in which FRCM coupons are extracted by cutting a larger panel [33], in this experimental campaign specific formworks were realized for the individual coupons thus minimizing the uncertainties related to the fabric reinforcement area per specimen. A first layer of fresh mortar (thickness 5 mm) was poured within metal molds (that are preliminarily sprayed with a lubricating oil to facilitate demolding) as illustrated in Figure 4, then the fabric was positioned, a gentle pressure was exerted to facilitate the adhesion between reinforcement textile and fresh cement paste, and finally a second layer of fresh mortar (thickness 5 mm) was poured to finish the coupon. Considering the width of the coupon and the yarn spacing of the employed fabrics, 2 yarns of basalt fabric, 3 yarns of carbon fabric, and 18 steel wires were involved in the cross-section of the FRCM coupon.

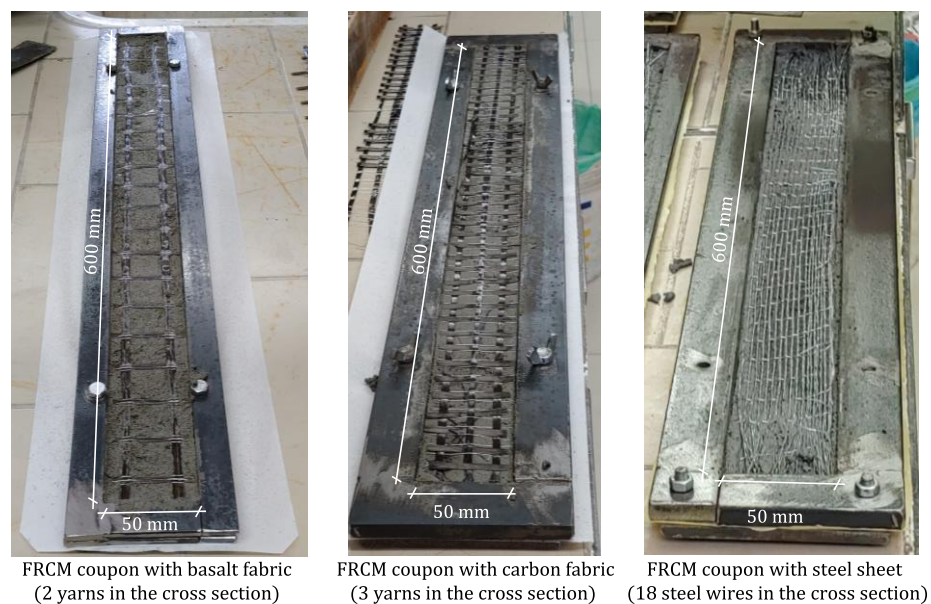


Figure 4. Preparation of FRCM coupons with basalt, carbon, and steel fibers.

For the prismatic specimens without fabric used to determine the tensile properties of the plain matrices, the same preparation procedure was followed by directly pouring the entire thickness (10 mm) of fresh mortar paste within the molds in a single phase. The coupons were demolded after 48 h and left to cure at controlled temperature ( $22 \pm 0.5 \text{ }^\circ\text{C}$ ) and humidity conditions (60%) for 28 days.

#### 2.4. FRCM Coupons: Tensile Test Setup and Measured Quantities

Steel tabs were bonded to the external faces of the coupons at the hardened state (i.e., after 28 days from casting) through a high-temperature-resistant, low-viscosity epoxy adhesive applied to both the mortar face and the steel plate, as shown in Figure 5.



**Figure 5.** FRCM coupons at the hardened state with steel tabs bonded with epoxy adhesive.

This special adhesive (two parts, resin and hardener) has the following characteristics: modified amine as hardener, fixture time (to develop a shear strength of 0.1 MPa at  $22 \text{ }^\circ\text{C}$ ) equal to 75 min, complete cure time 3 days at room temperature, shear strength 20 MPa cured for 7 days at  $22 \text{ }^\circ\text{C}$ , tensile strength (ISO 527-3) 31 MPa, tensile modulus (ISO 527-3) 6.7 GPa, compressive strength (ISO 604) 80 MPa determined on 1.2 mm thick samples.

All the tensile tests on the FRCM coupons were performed within a time frame of 7 days from one another to ensure a consistent comparison between specimens prepared with different matrices or fabrics but having a similar curing time. The tensile load was transferred from the testing machine to the FRCM coupons through the aforementioned steel tabs, 2.5 mm thick, epoxy bonded along the two terminal zones of the coupon for the entire width. It is well known from the literature that the contact length between steel tabs and FRCM coupon (also called “gripping length”) plays a key role in the mechanical characterization of the system through clevis-grip tensile tests [34,35]. A minimum gripping length of 75 mm is recommended by the US guidelines AC434 [28]. Some studies indicated that a contact length at least higher than 150 mm could be adequate for the complete characterization of different FRCM systems made of polyparaphenylene benzobisoxazole (PBO) dry fabric as well as dry and pre-impregnated carbon and basalt fabrics [33], although general estimations of the effective bond length of FRCM systems are hard to make. Based on these literature findings, a contact length equal to 165 mm (free length of 270 mm) was selected in this experimental campaign, as illustrated in Figure 6.

A clevis-grip system constituted by a clevis pin with diameter  $\text{Ø}20 \text{ mm}$  and an auxiliary steel plate in between the two steel tabs bonded to the specimen was used to apply shear stress without any normal stress, according to the clevis-grip tensile test setup in Figure 1. The auxiliary steel plate (and not the steel tabs bonded to the FRCM coupon) was clamped in the hydraulic wedges of the testing equipment through the wedges standard

clamping pressure. From a mechanical perspective, this test method aims at simulating a retrofitting condition in which the composite system is not anchored at its ends so that the response depends on the bond behavior at the fabric–matrix interface [26]. Tensile rupture of the fabric or fabric–matrix slippage are the two possible failure mechanisms.

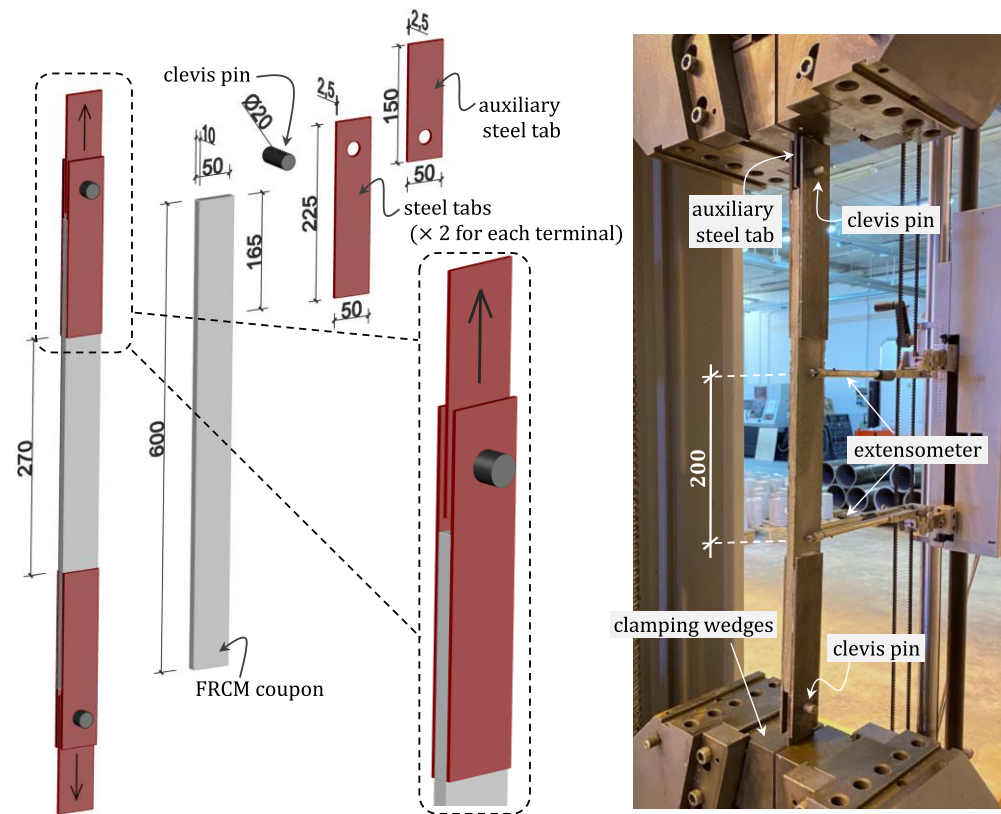


Figure 6. Dimensions (units in [mm]) and photograph of the clevis-grip tensile test configuration.

Monotonic tensile tests were performed in displacement control mode (0.2 mm/min according to [32]) through a universal testing machine (Zwick/Roell Z600) equipped with a 600 kN load cell and an initial preload of less than 5% of the expected ultimate load was applied to fully engage the clevis grip mechanism. Axial force ( $F$ ) was recorded by the integrated load cell of the testing machine, while the axial strain ( $\epsilon$ ) was measured through a 200 mm gauge length macro extensometer (see again Figure 6). When significant cracks fell beyond the gauge length of the extensometer, an approximate estimate of the strain was calculated as the global displacement of the crosshead (measured through a potentiometer integrated within the load cell) divided by the free length of the specimen, under the assumption that no slip occurs within the gripping length (the validity of this assumption has been checked a posteriori for all tested FRCM coupons). It is worth noting that a detailed discussion of possible strain measurements and their effects in clevis-grip tests has recently reported by Focacci et al. [36].

The force was normalized with reference to the cross-section of the fabric in the loading direction, depending on the number of yarns and the fabric thickness, to obtain the fabric axial stress  $\sigma_f$  as follows:

$$\sigma_f = \frac{F}{b_f \cdot t_f} \tag{1}$$

where  $b_f$  and  $t_f$  are the width and equivalent thickness of the fabric. It is worth noting that, according to the sketch in Figure 7, the modulus of elasticity changes from the uncracked to the cracked phase. The modulus of elasticity in the uncracked phase is termed  $E_f^* = \sigma_t / \epsilon_t$  ( $\sigma_t$  and  $\epsilon_t$  being the stress and strain associated with the first mortar cracking, corresponding

to the so-called transition point in Figure 7), while that in the cracked phase, termed  $E_f$  (Figure 7), is calculated according to AC434 provisions [28] as the secant slope between  $0.6\sigma_{fu}$  and  $0.9\sigma_{fu}$ :

$$E_f = \frac{0.3\sigma_{fu}}{\varepsilon_{f@0.9\sigma_{fu}} - \varepsilon_{f@0.6\sigma_{fu}}} \quad (2)$$

where  $\sigma_{fu}$  is the ultimate tensile strength of the FRCM coupon, while  $\varepsilon_{f@0.6\sigma_{fu}}$  and  $\varepsilon_{f@0.9\sigma_{fu}}$  are the strains corresponding to  $0.6\sigma_{fu}$  and  $0.9\sigma_{fu}$  in the stress–strain curve, respectively. It is worth noting that  $E_f$  includes both the elastic deformation of the fabric and its slippage within the matrix occurring in the post-cracking phase. In compliance with AC434 provisions [28], the ultimate tensile strain  $\varepsilon_{fu}$  for the FRCM coupons was calculated by extrapolation of the secant slope  $E_f$  up to the stress level  $\sigma_{fu}$ , which in mathematical form is expressed as:

$$\varepsilon_{fu} = \varepsilon_{f@0.6\sigma_{fu}} + \frac{0.4\sigma_{fu}}{E_f} \quad (3)$$

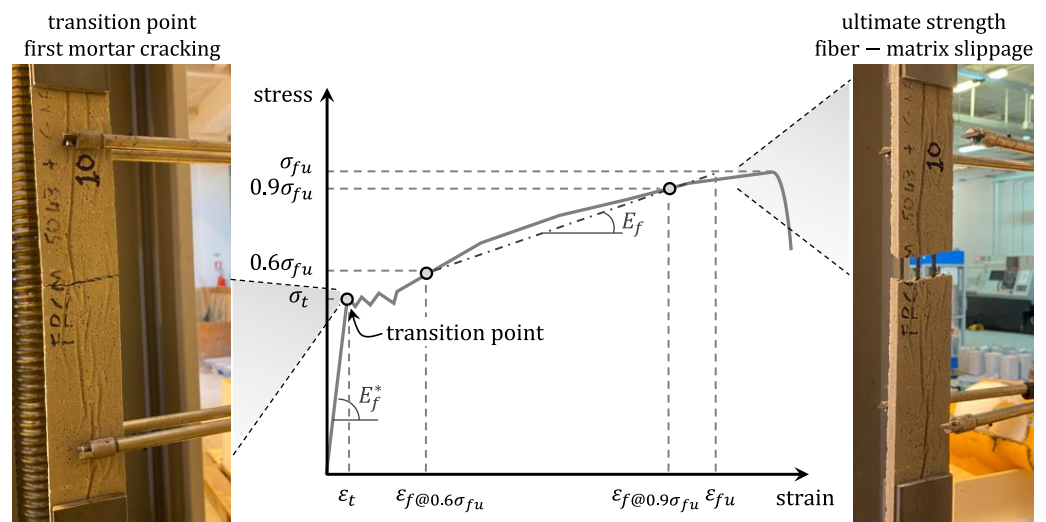


**Figure 7.** Schematic results of clevis-grip tensile tests and identification of characteristic points and mechanical parameters according to AC434 guidelines [28].

Finally, the determination of the tensile stress in the prismatic coupons without fabric  $\sigma_{matrix}$  was performed through the following equation:

$$\sigma_{matrix} = \frac{F}{b_0 \cdot t} \quad (4)$$

where  $b_0$  and  $t$  represent the nominal width and thickness of the prismatic specimen, respectively. The ultimate strain is here assumed as the strain value attained at the peak value of  $\sigma_{matrix}$  in the stress–strain curve. This matrix axial stress was additionally computed for FRCM coupons and reported along a secondary vertical axis in order to investigate the matrix’s contribution in the overall tensile behavior of the specimen for the various investigated cement-based matrices.

### 3. Results and Discussion

Before testing the FRCM coupons (realized with various fabrics and matrices), clevis-grip tensile tests are performed on prismatic specimens (same nominal dimensions as reported in Section 2.3) without fabrics in order to investigate the tensile properties of the plain matrices. Three coupons per composite are realized, although in some cases the results of just two replications per type are reported because some specimens, especially

the coupons without fabrics, exhibited micro-cracking before testing, probably due to the manufacturing process. Relevant results are illustrated in Figure 8 in terms of stress–strain curves (left) and stiffness and strength indicators (right): it is clearly seen that the tensile behavior obtained from these tests is consistent with the mechanical properties of the three matrices in Figure 3. In particular, matrix C exhibits the best mechanical performance in terms of elastic modulus and tensile strength, whereas matrices A and B show relatively comparable results, around 20% lower than matrix C. The tensile strength ranges from 1.5 to 2.5 MPa, depending on the matrix. The failure mode observed for all these (plain matrix) specimens is brittle, and the tests are stopped once the matrix starts cracking. These results are useful to interpret the composite behavior of the FRCM coupons, as clarified below.

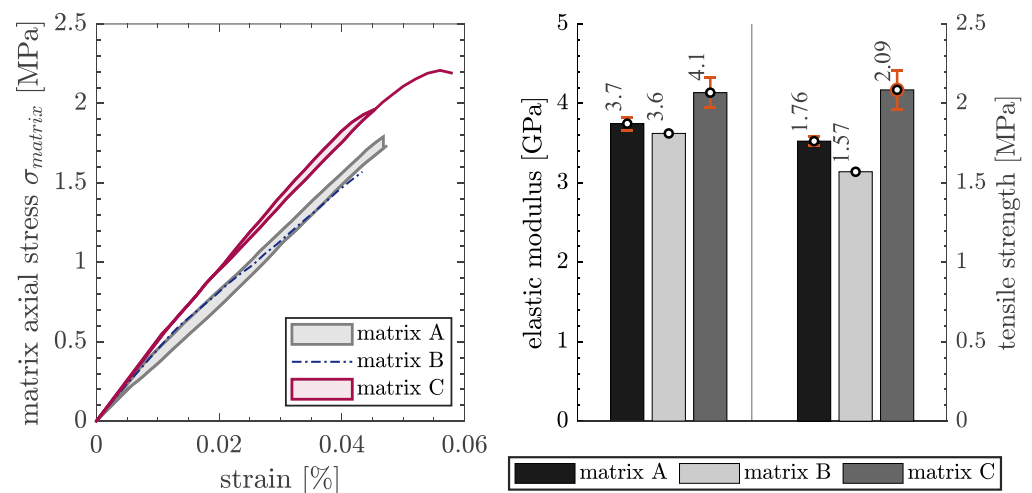


**Figure 8.** Stress–strain curves (left) and elastic modulus and tensile strength (right) of prismatic specimens realized with three different cement-based matrices without fabrics (plain matrix).

The stress–strain curves for the basalt, carbon, and steel FRCM coupons realized with the three cement-based matrices are illustrated in Figure 9. The basalt and carbon curves, especially those relevant to matrix C, clearly show the typical three-phase trend observed in FRCM tensile tests and alternative clamping-grip configurations [23]: In the first phase, the load is mainly resisted by the matrix until the matrix tensile strength is attained. Subsequently, load drops are observed corresponding to the formation of multiple cracks along the FRCM coupon (second stage). Finally, in the third phase, matrix crack saturation takes place and the applied load is mainly resisted by the reinforcement fabric and increases progressively until failure (the test is stopped when the load decreases of more than 80% compared to the maximum recorded load).

By looking at the axis scale of the secondary  $y$ -axis reported in the plots, the transition point (corresponding to the first mortar cracking) of all the stress–strain curves is associated with a value of  $\sigma_{matrix}$  in the range 1–3 MPa, slightly variable depending on the matrix employed: these stress values are consistent with the expected matrix tensile strength resulting from the measured flexural strength (assuming, as preliminary estimate, matrix tensile strength equal to half of the corresponding matrix flexural strength in Figure 3, according to Model Code 2010 formulation [24,37]) and with the clevis-grip tensile test results on the plain matrices reported in Figure 8. The difference observed in the stress values among the three matrices in the first stage of loading clearly indicates the dominant role of the matrix mechanical characteristics on the FRCM coupon initial tensile behavior. The matrix C is associated with the highest stress value in the transition point  $\sigma_t$  for all fabrics studied, which inherently results from the highest value of the matrix flexural strength in Figure 3, and, consequently, the highest matrix tensile strength  $\sigma_{matrix}$ . Not only in the pre-cracked phase, but also in the cracked phase, matrix C shows the best mechanical performance in terms of FRCM coupon tensile strength  $\sigma_f$  (for all fabrics) and

ultimate tensile strain  $\epsilon_{fu}$  (for all but one case, i.e., basalt FRCM), which indicates a very good compatibility behavior at the fabric–matrix interface that makes it possible to exploit the tensile properties of the reinforcement mesh to a relatively large extent. This suggests that matrix C could be indicated as the most suitable candidate to optimize the interfacial stress transfer at the fiber–matrix interface thus exalting the mechanical performances of the composite system.

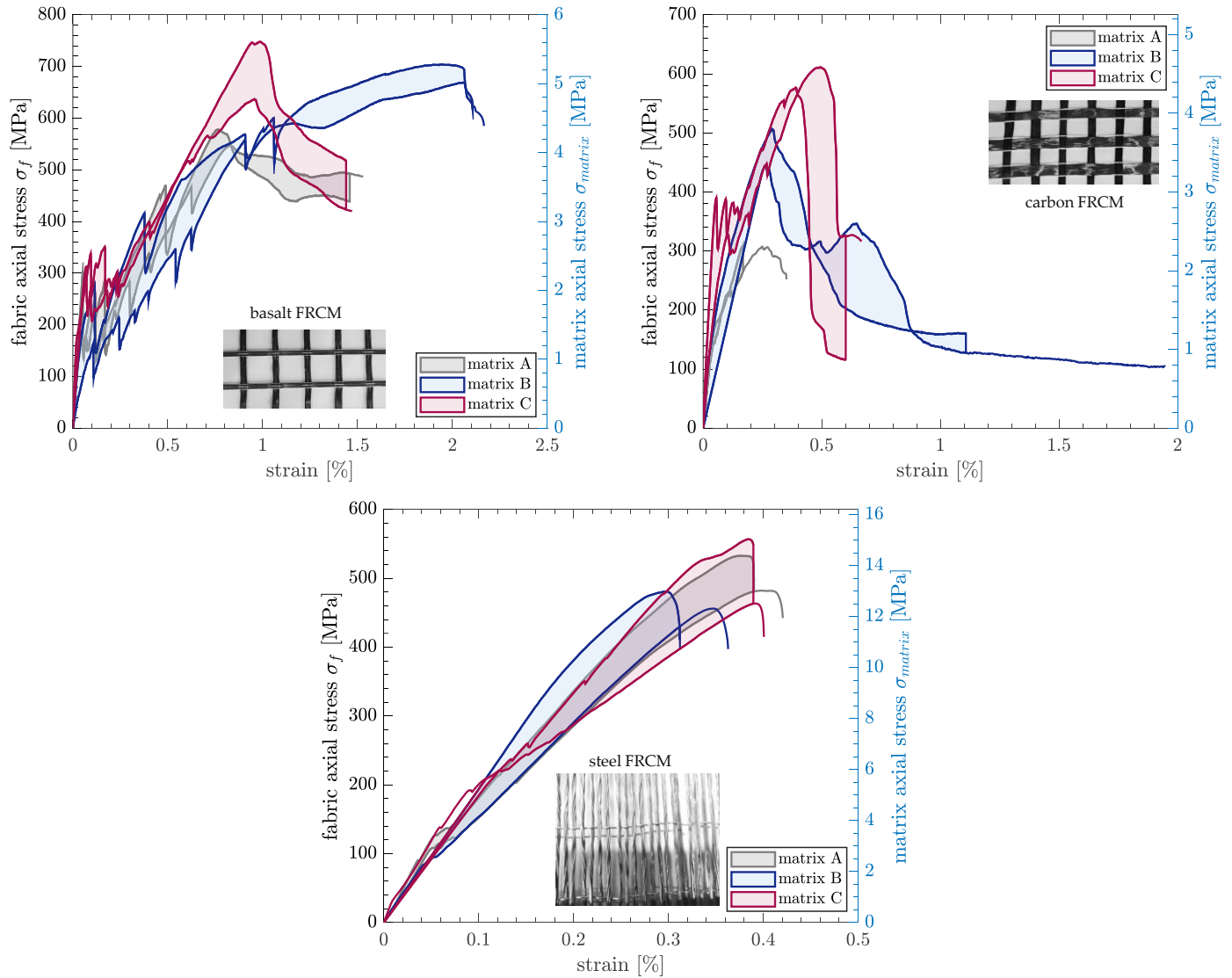


**Figure 9.** Stress–strain curves of basalt, carbon, and steel FRCM coupons realized with different cement-based matrices.

Further considerations can be argued comparing the stress–strain curves by varying the fabric material type. It is possible to observe a more marked stress drop for the basalt and carbon FRCM coupons than the steel FRCM coupons, which is symptomatic of a significantly lower amount of fabric reinforcement area (compare again the surface mesh density listed in Table 1 for the three fabrics studied) that is not enough to absorb the energy released as soon as the matrix cracking occurs, as was also observed in other literature studies [26,33]. The difference in the transition between the uncracked and cracked stage of the different composites could also be due to the different matrix–textile bond behaviors. On the contrary, a narrow stress plateau (rather than a sudden stress drop) can be observed in the steel FRCM coupons after the first mortar cracking, which confirms that the energy released in this case is fully absorbed by the UHTSS steel cords due to the higher fabric

density of the steel reinforcement, which is indeed one order of magnitude higher than the basalt and carbon density surface density. The scatter of the stress–strain curves of the tested coupons in Figure 9 is reasonably in line with other tensile tests of FRCM composites from the literature [24,26] and might be attributed to chaotically distributed micro-defects within the cement-based matrix (for the variability of the curves observed in the first stage of the loading process) and to the random occurrence of multiple matrix micro-cracks not always falling within the gauge of the extensometer (for the variability of the curves in the second and third stages of the loading process).

With regard to the failure mechanisms, the failure is either ascribed to complete fiber slippage within the matrix (for basalt and carbon FRCM, see Figures 10 and 11) or to mortar splitting in the gripped part of the specimen (for steel FRCM, see Figure 12). In particular, for both basalt and carbon FRCM, once the crack pattern becomes stable (i.e., no new cracks develop), the increasing axial strain resulting from the imposed displacement is allowed by further crack opening and fiber slippage within the matrix. Therefore, the tensile behavior of basalt and carbon FRCM is mainly related to the bond performance at the fabric–matrix interface.

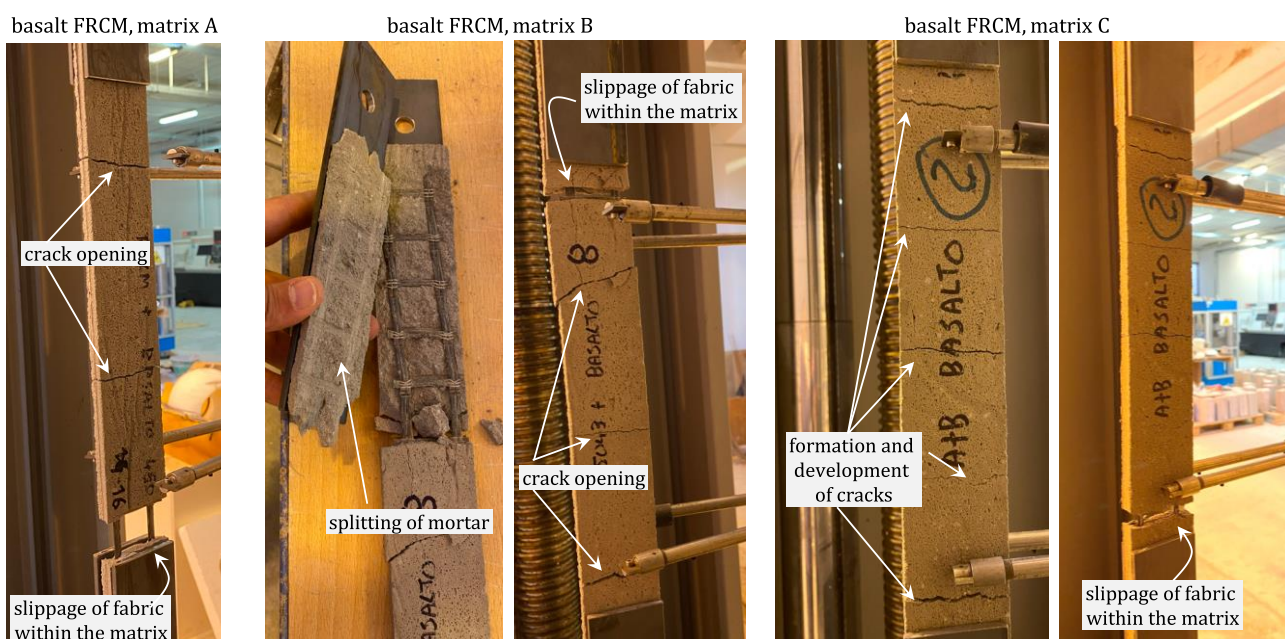


**Figure 10.** Failure mechanisms of basalt FRCM coupons realized with different cement-based matrices.

As shown in Figure 10, the number of cracks in the basalt FRCM for all the studied matrices is generally larger than in the carbon FRCM coupons (cf. Figure 11), which is consistent with the numerous stress drops beyond the transition point in the corresponding stress–strain curves. For some specimens realized with matrix B, splitting of mortar within the gripping length of the basalt FRCM coupons is also observed. In general, the pre-impregnation of the basalt fabric allows for a relatively large ultimate strain of the FRCM coupons (>1%) resulting from the good bond behavior at the fabric–matrix interface compared to the carbon and steel fabrics, which is in line with the higher values of the fabric ultimate strain reported in Table 1.

In the carbon FRCM coupons (Figure 11), the failure typically occurs with one main matrix crack from which fiber slippage is triggered for matrix A and B, whereas multiple cracks develop for matrix C, which indeed corresponds to multiple stress drops in the corresponding stress–strain curves in Figure 9. In the latter case (matrix C), despite the higher value of tensile strength, the fiber exploitation ratio is still relatively low (a value of tensile strength of the carbon FRCM coupons of around 500–600 MPa is attained, much lower than the theoretical fabric tensile strength equal to 1850 MPa as reported in Table 1)

because the fiber filaments within each yarn are plausibly subjected to a non-homogeneous stress distribution.

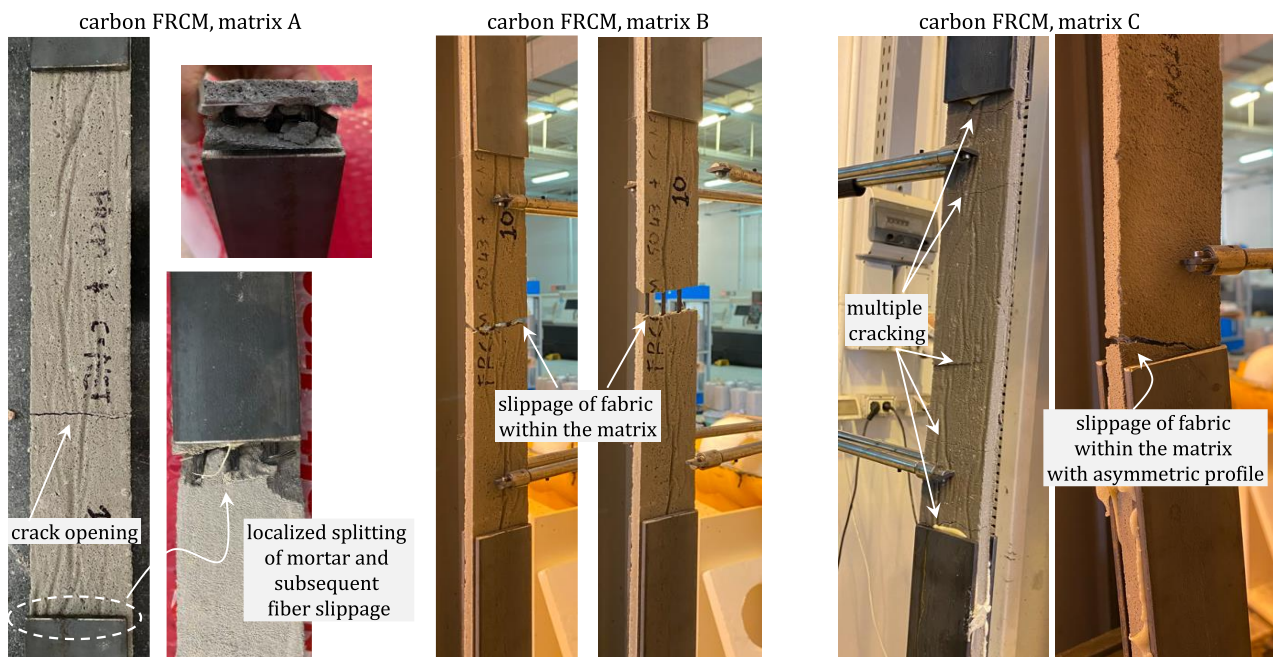


Figure 11. Failure mechanisms of carbon FRCM coupons realized with different cement-based matrices.

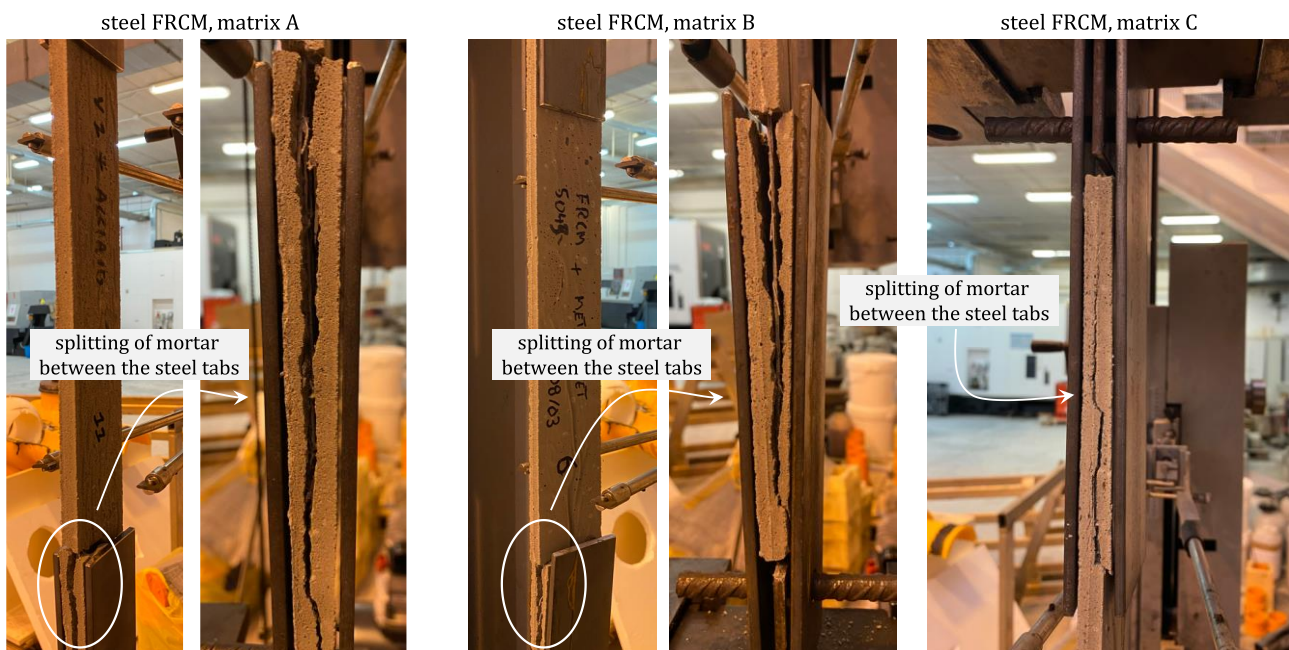


Figure 12. Failure mechanisms of steel FRCM coupons realized with different cement-based matrices.

More specifically, for carbon FRCM coupons realized with matrix C, after the formation and development of multiple cracks along the free portion of the specimen, slippage of fabric takes place and in some cases, the specimen fails with an asymmetric profile, as depicted in Figure 11, which indicates an uneven stress distribution among various fiber filaments and among different yarns. This undesired behavior, often noted in the literature for other dry (i.e., not pre-impregnated) fiber textiles such as PBO composites [24], can be explained by considering that the matrix impregnates more easily the external (sleeve)

fiber filaments of the single yarn, while leaving the internal (core) ones in a dry form. This heterogeneous degree of impregnation of the fiber yarns gives rise to a telescopic failure of the carbon filaments, lowering the overall tensile strength of the carbon fabric. To avoid this uneven stress distribution among the fiber filaments within each yarn, in the literature carbon textiles for FRCM systems were also used in their “coated” version, i.e., by fully pre-impregnating the fiber filaments with a flexible epoxy resin combined with a layer of quartz sand [33] through different levels of pre-impregnation (light, medium, and high) [16] or using other epoxy-based impregnation agents [31].

On the contrary, for steel FRCM, the failure (illustrated in Figure 12) is ascribed to the splitting of the mortar due to longitudinal cracks in the gripping area with minimal fabric slippage within the matrix, which inherently suggests a better bond performance between the UHTSS steel cords and the surrounding matrix. The very high fiber density of the UHTSS steel cords exert a high shear bond stress at the fabric–matrix interface, thus forming a rupture surface parallel to the primary direction of the fabric, as was similarly observed in other works from the literature [26]. Therefore, for steel FRCM coupons, it is the quality of the mortar (rather than the fabric characteristics) that influences not only the ultimate behavior, but also the stiffness of the FRCM coupon in the uncracked and cracked phases through a progressive widening of the longitudinal cracks in the gripping area (although in this case it might be not appropriate to identify these two phases, considering the absence of a clear transition point in Figure 9).

Even though few replications (two–four, depending on the case) of identical specimens are considered (certainly less than the minimum number of tests required for rigorous acceptance methods [26,32]), it is interesting to compute the mean values (along with pertinent error bars) of the mechanical parameters introduced in Section 2.4, which represent indicators of the stiffness, strain, and stress tensile response of the FRCM coupons [38,39]. The histograms of such parameters are shown in Figure 13 for all the tested FRCM coupons. As intuitively observed through the stress–strain curves, the stiffness characteristics of the specimens (both in the uncracked,  $E_f^*$ , and cracked,  $E_f$ , phase) are not significantly affected by the selection of a specific matrix, while they are sensibly influenced by the kind of fabric employed. Indeed, there is no clear trend in the values of tensile moduli calculated on FRCM coupons prepared with the same fabric but using different mortar matrices—the differences of  $E_f^*$  are relatively high only for basalt FRCM coupons, and are limited to within a  $\pm 15\%$  range for the carbon and steel FRCM coupons.

A common quality observed in the three kinds of fabrics is that the lowest uncracked tensile modulus  $E_f^*$  is obtained for matrix B, which is consistent with the fact that this matrix is indeed associated with the lowest value of flexural strength among the three studied matrices, as reported in the previous Figure 3. This result confirms that the stiffness in the first stage of loading (up to the transition point) is mainly influenced by the properties of the mortar matrix. In the case of clamping-grip tensile tests, the value of cracked elastic modulus  $E_f$  should be, in principle, consistent with the bare fiber elastic modulus [23] (in a hypothetical scenario in which the matrix is fully cracked, the contribution of the matrix would be negligible). On the other hand, in the clevis-grip tensile tests, matrix–textile slippage may occur within the gripped length. This is why the measured cracked elastic modulus  $E_f$  can be lower than that of the bare fabric. According to this explanation, the values of  $E_f$  experimentally measured in the basalt and carbon FRCM coupons and reported in Figure 13 are slightly lower than the elastic moduli of the corresponding bare fabrics, which is also plausibly due to the fact that the bundles are not undergoing a uniform stress state and that fabric–matrix slippage governs the tensile behavior in most cases. Additionally, the secant slope is also marginally influenced by a residual stiffness contribution of the cracked mortar (i.e., crack bridging effects, friction and interlocking at the fabric–matrix interface, etc.). The measured elastic moduli in the uncracked and cracked phase for the steel FRCM coupons are relatively close to each other, which is due to the absence of a clear transition point in the stress–strain curves.

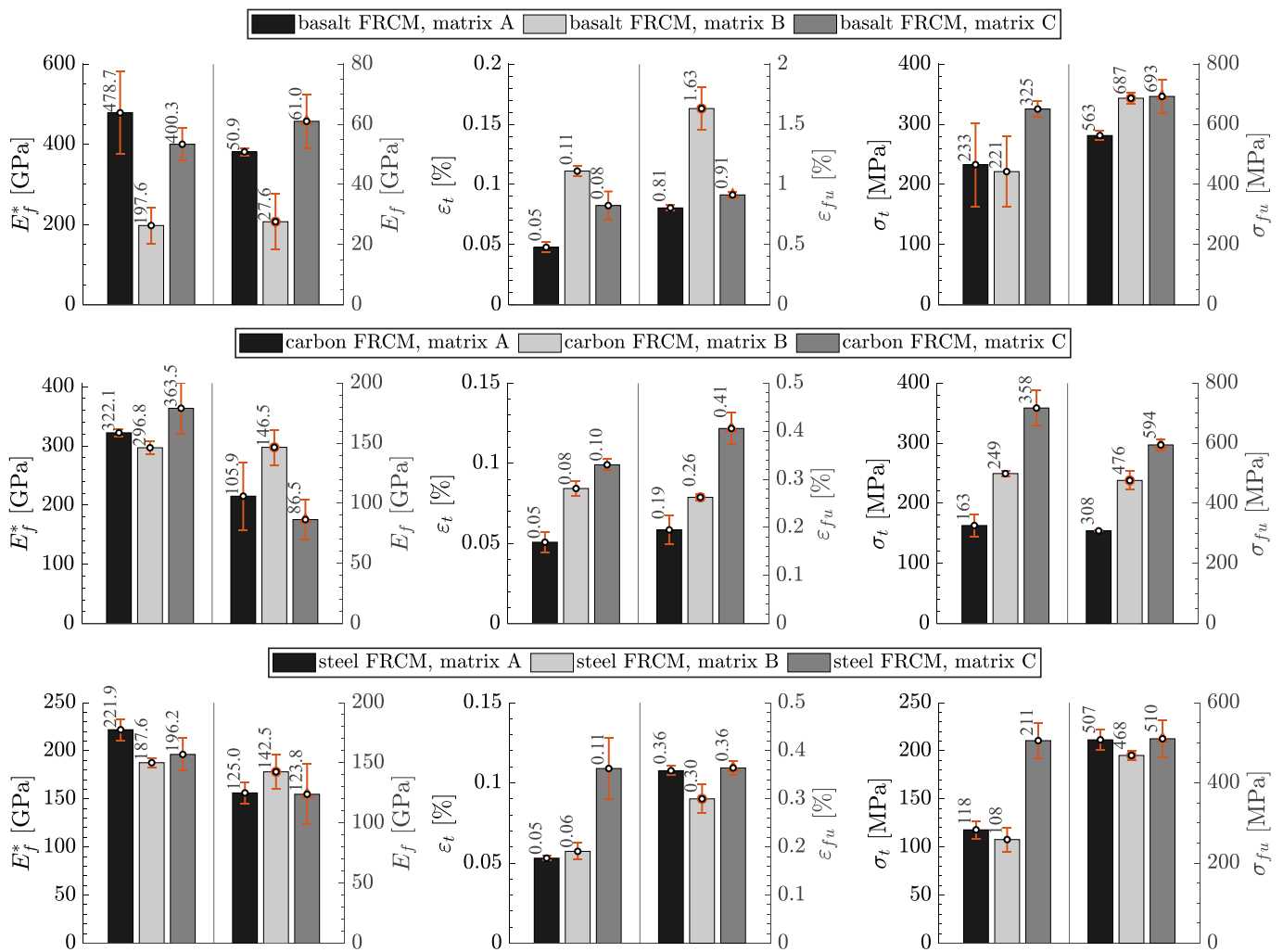


**Figure 13.** Uncracked ( $E_f^*$ ) and cracked ( $E_f$ ) elastic modulus (left), tensile strain (center) and tensile stress (right) at the transition point ( $\epsilon_t$  and  $\sigma_t$ , respectively) and at ultimate conditions ( $\epsilon_{fu}$  and  $\sigma_{fu}$ , respectively) of FRCM coupons realized with different fabrics and cement-based matrices.

With regard to the strain response, the strain at the transition point  $\epsilon_t$  falls in the range 0.05–0.11% for the three fabrics, and its value is related to the matrix employed. In matrix A, the mortar cracking occurs at lower strain values than in matrices B and C, and matrix C is associated with the largest values of  $\epsilon_t$  and  $\epsilon_{fu}$  for carbon and steel FRCM. A very good compatibility behavior is observed between matrix B and basalt fabric, with ultimate strain values >1.5%, corresponding to the splitting of mortar within the gripping area of the specimen (cf. again Figure 10). However, for the three fabrics, the ultimate strains  $\epsilon_{fu}$  (in general characterized by a lower dispersion value than the elastic moduli) are much lower than the ultimate strain capacity of the bare fabric, as the test is stopped when the fabric–matrix slippage becomes excessive, sometimes causing localized rotation or parasitic out-of-plane movements of the steel tabs. With regard to the stress response, as anticipated above, the two-component matrix C exhibits the best performance in terms of tensile strength  $\sigma_{fu}$  for the three considered fabrics, whereas the behavior of the one-component matrices A and B is relatively comparable for steel FRCM. For basalt and carbon FRCM, the matrix B exhibits a superior performance than the matrix A in terms of ultimate tensile strength  $\sigma_{fu}$  for basalt and carbon FRCM (+22% and +54%, respectively).

#### 4. Conclusions and Future Perspectives

Clevis-grip tensile tests on FRCM systems realized with customized matrices, ad hoc developed in this work, have been presented. The FRCM systems investigated in this paper are fabricated with three matrices characterized by a different mix design and prepared with three different resins/binders, namely one-component mortar incorporating dispersible copolymer powder of vinyl acetate and ethylene (matrix A and B) or two-component mortar with liquid resin of carboxylated styrene–butadiene copolymer (matrix C). Three fabrics, namely basalt pre-impregnated textile, carbon dry fiber rovings, and ultra-high strength steels galvanized wires twisted in cords, were investigated. This made it possible to identify the most suitable resin/binder for improving the adhesion between the cementitious matrix and the fabric.

The main findings of this research work can be summarized as follows:

1. With regard to the mechanical characteristics of the matrices, matrix C exhibits a lower performance than matrix A in the early curing times (3 days) but better mechanical behavior during the development of the hardening process (+20% and +30% at 7 and 28 days in terms of flexural strength, +33% at 28 days in terms of compression strength). Matrix B exhibits the worst performance among the three considered matrices at 28 days, with strength results slightly lower than those of matrix A.
2. With regard to the stress–strain curves, the basalt and carbon FRCM coupons show a three-phase trend, similar to what is observed in alternative clamping-grip tensile tests from the literature: in the first phase, the load is mainly resisted by the matrix until the matrix tensile strength is attained; subsequently, load drops are observed corresponding to the formation of multiple cracks along the FRCM coupon; finally, in the third phase, matrix crack saturation takes place and the applied load is mainly resisted by the reinforcement fabric and increases progressively until failure. On the contrary, a stress plateau (rather than a sudden stress drop) is observed in the steel FRCM coupons after the first mortar cracking (transition point), which confirms that the energy released is fully absorbed by the UHTSS steel cords due to the higher fabric density of the steel reinforcement than the basalt and carbon fabrics.
3. The matrix tensile stress in the first stage of loading clearly indicates the dominant role of the matrix mechanical characteristics on the FRCM coupon initial tensile behavior. Matrix C is associated with the highest stress value in the transition point  $\sigma_t$  for all fabrics studied, which inherently results from the highest value of the matrix flexural strength. Not only in the pre-cracked phase, but also in the cracked phase the matrix C shows the best mechanical performance in terms of FRCM coupon tensile strength  $\sigma_f$  (for all fabrics) and ultimate tensile strain  $\varepsilon_{fu}$  (for all but one case, i.e., basalt FRCM), which indicates a very good compatibility behavior at the fabric–matrix interface. For basalt and carbon FRCM, the matrix B exhibits a superior performance than matrix A in terms of ultimate tensile strength  $\sigma_{fu}$  for basalt and carbon FRCM (+22% and +54%, respectively).
4. The failure for basalt and carbon FRCM is ascribed to complete fiber slippage within the matrix: therefore, the tensile behavior of basalt and carbon FRCM mainly relies on the bond performance at the fabric–matrix interface. A very good compatibility behavior is observed between matrix B and basalt fabric, with ultimate strain values >1.5% corresponding to the splitting of mortar within the gripping area of the specimen. In carbon FRCM coupons, the failure typically occurs with one main matrix crack from which fiber slippage is triggered for matrix A and B, whereas multiple cracks develop for matrix C, which indeed corresponds to multiple stress drops in the corresponding stress–strain curves. In some cases, slippage of carbon fabric takes place with an asymmetric profile because the fiber filaments within each yarn are plausibly subjected to a non-homogeneous stress distribution considering that the cement-based matrix impregnates more easily the external (sleeve) fiber filaments of the single yarn while leaving the internal (core) ones in a dry form. On the contrary, for steel FRCM, the failure is ascribed to the splitting of the mortar due to longitudinal

cracks in the gripping area, with minimal fabric slippage within the matrix, which suggests a better bond performance between the UHTSS steel cords and the surrounding matrix. Therefore, for steel FRCM coupons, it is the quality of the mortar (rather than the fabric characteristics) that influences not only the ultimate behavior but also the stiffness of the FRCM coupon in the uncracked and cracked phase.

In the authors' opinion, the experimental findings reported in this paper can be useful for designing optimized mortar mixes aimed at realizing novel FRCM composites or at improving existing FRCM systems, by suitably accounting for compatibility behavior and slippage at the fabric–matrix interface. For a complete characterization of the FRCM systems of this experimental campaign, the tensile test results will be complemented, in a forthcoming article, with double-lap shear bond tests performed on different substrates (concrete, tuff, and clay bricks) to investigate the occurrence of other potential failure modes (i.e., cohesive debonding within the substrate and detachment at the FRCM–substrate interface [26]) and to determine appropriate conventional stress and strain values [27] for designing strengthening interventions on existing structures.

**Author Contributions:** Conceptualization, D.D.D., N.M., P.L., G.R. and G.G.; methodology, D.D.D., N.M., P.L., G.R. and G.G.; software, D.D.D., N.M. and P.L.; validation, D.D.D., N.M., P.L., G.R. and L.C.; formal analysis, D.D.D., N.M. and P.L.; investigation, D.D.D., N.M., P.L. and L.C.; data curation, D.D.D., N.M. and P.L.; writing—original draft preparation, D.D.D.; writing—review and editing, D.D.D., N.M. and L.C.; supervision, G.R. and L.C.; funding acquisition, L.C. All authors have read and agreed to the published version of the manuscript.

**Funding:** This research was funded by the P.O. FESR Sicilia 2014/2020 (Axis 1, Action 1.1.5 “Support for the technological advancement of companies through the financing of pilot lines and actions for early validation of products and large-scale demonstrations”) Project 082030000276 SMART-ART “Sviluppo di metodi avanzati di restauro, diagnostica e telecontrollo per la conservazione del patrimonio artistico architettonico”, CUP G79J18000620007.

**Institutional Review Board Statement:** Not applicable.

**Informed Consent Statement:** Not applicable.

**Data Availability Statement:** Data sharing not applicable.

**Acknowledgments:** The authors would like to thank the technical support of the company Tradimalt S.p.A. (Messina, Italy) and the company G&P Intech (Altavilla Vicentina, Italy) for providing the mortars and fabrics used in this experimental campaign.

**Conflicts of Interest:** The authors declare no conflict of interest.

## References

1. ACI Committee 549. *ACI 549.6R-20 Guide to Design and Construction of Externally Bonded Fabric-Reinforced Cementitious Matrix (FRCM) and Steel-Reinforced Grout (SRG) Systems for Repair and Strengthening Masonry Structures*; American Concrete Institute: Farmington Hills, MI, USA, 2020.
2. Carozzi, F.G.; Bellini, A.; D'Antino, T.; De Felice, G.; Focacci, F.; Hojdys, Ł.; Laghi, L.; Lanoye, E.; Micelli, F.; Panizza, M.; et al. Experimental investigation of tensile and bond properties of Carbon-FRCM composites for strengthening masonry elements. *Compos. Part B Eng.* **2017**, *128*, 100–119. [[CrossRef](#)]
3. ACI Committee 440.2R-17. *Guide for the Design and Construction of Externally Bonded FRP Systems for Strengthening Concrete Structures*; American Concrete Institute: Farmington Hills, MI, USA, 2017.
4. De Domenico, D.; Fuschi, P.; Pardo, S.; Pisano, A. Strengthening of steel-reinforced concrete structural elements by externally bonded FRP sheets and evaluation of their load carrying capacity. *Compos. Struct.* **2014**, *118*, 377–384. [[CrossRef](#)]
5. De Felice, G.; Aiello, M.A.; Caggegi, C.; Ceroni, F.; De Santis, S.; Garbin, E.; Gattesco, N.; Hojdys, Ł.; Krajewski, P.; Kwiecień, A.; et al. Recommendation of RILEM Technical Committee 250-CSM: Test method for Textile Reinforced Mortar to substrate bond characterization. *Mater. Struct.* **2018**, *51*, 95. [[CrossRef](#)]
6. Faleschini, F.; Zanini, M.A.; Hofer, L.; Toska, K.; De Domenico, D.; Pellegrino, C. Confinement of reinforced concrete columns with glass fiber reinforced cementitious matrix jackets. *Eng. Struct.* **2020**, *218*, 110847. [[CrossRef](#)]
7. Ombres, L. Concrete confinement with a cement based high strength composite material. *Compos. Struct.* **2014**, *109*, 294–304. [[CrossRef](#)]

8. Raoof, S.M.; Koutas, L.N.; Bourmas, D.A. Textile-reinforced mortar (TRM) versus fibre-reinforced polymers (FRP) in flexural strengthening of RC beams. *Constr. Build. Mater.* **2017**, *151*, 279–291. [CrossRef]
9. De Domenico, D. RC members strengthened with externally bonded FRP plates: A FE-based limit analysis approach. *Compos. Part B Eng.* **2015**, *71*, 159–174. [CrossRef]
10. Bencardino, F.; Carloni, C.; Condello, A.; Focacci, F.; Napoli, A.; Realfonzo, R. Flexural behaviour of RC members strengthened with FRCM: State-of-the-art and predictive formulas. *Compos. Part B Eng.* **2018**, *148*, 132–148. [CrossRef]
11. Gonzalez-Libreros, J.; Sneed, L.; D’Antino, T.; Pellegrino, C. Behavior of RC beams strengthened in shear with FRP and FRCM composites. *Eng. Struct.* **2017**, *150*, 830–842. [CrossRef]
12. Marcinczak, D.; Trapko, T.; Musiał, M. Shear strengthening of reinforced concrete beams with PBO-FRCM composites with anchorage. *Compos. Part B Eng.* **2018**, *158*, 149–161. [CrossRef]
13. D’Antino, T.; Focacci, F.; Sneed, L.H.; Pellegrino, C. Shear Strength Model for RC Beams with U-Wrapped FRCM Composites. *J. Compos. Constr.* **2020**, *24*, 04019057. [CrossRef]
14. Hegger, J.; Will, N.; Rüberg, K. Textile reinforced concrete—A new composite material. In *Advances in Construction Materials*; Springer: Berlin/Heidelberg, Germany, 2007.
15. Ascione, L.; de Felice, G.; De Santis, S. A qualification method for externally bonded Fibre Reinforced Cementitious Matrix (FRCM) strengthening systems. *Compos. Part B Eng.* **2015**, *78*, 497–506. [CrossRef]
16. Donnini, J.; Corinaldesi, V.; Nanni, A. Mechanical properties of FRCM using carbon fabrics with different coating treatments. *Compos. Part B Eng.* **2016**, *88*, 220–228. [CrossRef]
17. Colombi, P.; D’Antino, T. Analytical assessment of the stress-transfer mechanism in FRCM composites. *Compos. Struct.* **2019**, *220*, 961–970. [CrossRef]
18. D’Antino, T.; Sneed, L.H.; Carloni, C.; Pellegrino, C. Effect of the inherent eccentricity in single-lap direct-shear tests of PBO FRCM-concrete joints. *Compos. Struct.* **2016**, *142*, 117–129. [CrossRef]
19. Sneed, L.; D’Antino, T.; Carloni, C.; Pellegrino, C. A comparison of the bond behavior of PBO-FRCM composites determined by double-lap and single-lap shear tests. *Cem. Concr. Compos.* **2015**, *64*, 37–48. [CrossRef]
20. De Domenico, D.; Urso, S.; Borsellino, C.; Spinella, N.; Recupero, A. Bond behavior and ultimate capacity of notched concrete beams with externally-bonded FRP and PBO-FRCM systems under different environmental conditions. *Constr. Build. Mater.* **2020**, *265*, 121208. [CrossRef]
21. De Domenico, D.; Quattrocchi, A.; Alizzio, D.; Montanini, R.; Urso, S.; Ricciardi, G.; Recupero, A. Experimental Characterization of the FRCM-Concrete Interface Bond Behavior Assisted by Digital Image Correlation. *Sensors* **2021**, *21*, 1154. [CrossRef]
22. Bertolesi, E.; Carozzi, F.G.; Milani, G.; Poggi, C. Numerical modeling of Fabric Reinforce Cementitious Matrix composites (FRCM) in tension. *Constr. Build. Mater.* **2014**, *70*, 531–548. [CrossRef]
23. Calabrese, A.S.; D’Antino, T.; Colombi, P.; Poggi, C. Low- and High-Cycle Fatigue Behavior of FRCM Composites. *Materials* **2021**, *14*, 5412. [CrossRef]
24. D’Antino, T.; Poggi, C. Characterization and Design of Multilayer PBO FRCM Composite Reinforcements for Concrete Structures. *J. Compos. Constr.* **2021**, *25*, 04021048. [CrossRef]
25. Focacci, F.; D’Antino, T.; Carloni, C. The role of the fiber–matrix interfacial properties on the tensile behavior of FRCM coupons. *Constr. Build. Mater.* **2020**, *265*, 120263. [CrossRef]
26. De Santis, S.; Hadad, H.A.; Basalo, F.D.C.Y.; de Felice, G.; Nanni, A. Acceptance Criteria for Tensile Characterization of Fabric-Reinforced Cementitious Matrix Systems for Concrete and Masonry Repair. *J. Compos. Constr.* **2018**, *22*, 04018048. [CrossRef]
27. National Research Council (CNR). *Istruzioni per la Progettazione, l’esecuzione ed il Controllo di Interventi di Consolidamento Statico Mediante l’utilizzo di Compositi Fibrorinforzati a Matrice Inorganica*; CNR-DT 215/2018; CNR: Rome, Italy, 2018.
28. AC434 Acceptance criteria for concrete and masonry strengthening using fabric-reinforced cementitious matrix (FRCM) composite Systems. *ICC Eval. Serv.* **2018**, *324*, 4–11.
29. Focacci, F.; D’Antino, T.; Carloni, C. Tensile Tests of FRCM Coupons: The Influence of the Fiber-Matrix Bond Properties. In *Proceedings of the International Conference on Fibre-Reinforced Polymer (FRP) Composites in Civil Engineering*, Istanbul, Turkey, 8–10 December 2021. [CrossRef]
30. Donnini, J.; Bompadre, F.; Corinaldesi, V. Tensile Behavior of a Glass FRCM System after Different Environmental Exposures. *Processes* **2020**, *8*, 1074. [CrossRef]
31. Nobili, A.; Signorini, C. On the effect of curing time and environmental exposure on impregnated Carbon Fabric Reinforced Cementitious Matrix (CFRCM) composite with design considerations. *Compos. Part B Eng.* **2017**, *112*, 300–313. [CrossRef]
32. Italian Guidelines: Consiglio Superiore dei Lavori Pubblici Linea Guida per la Identificazione, la Qualificazione ed il Controllo di Accettazione di Compositi Fibrorinforzati a Matrice Inorganica (FRCM) da Utilizzarsi per il Consolidamento Strutturale di Costruzioni Esistenti. Consiglio Superiore dei Lavori Pubblici, Servizio Tecnico Centrale, Rome, Italy, 2018. Available online: <https://www.reluis.it/images/normativa/Linea%20Guida%20Qualificazione%20FRCM.pdf> (accessed on 20 August 2022).
33. Donnini, J.; Corinaldesi, V. Mechanical characterization of different FRCM systems for structural reinforcement. *Constr. Build. Mater.* **2017**, *145*, 565–575. [CrossRef]
34. Arboleda, D.; Carozzi, F.G.; Nanni, A.; Poggi, C. Testing Procedures for the Uniaxial Tensile Characterization of Fabric-Reinforced Cementitious Matrix Composites. *J. Compos. Constr.* **2016**, *20*, 04015063. [CrossRef]

35. Contamine, R.; Larbi, A.S.; Hamelin, P. Contribution to direct tensile testing of textile reinforced concrete (TRC) composites. *Mater. Sci. Eng. A* **2011**, *528*, 8589–8598. [[CrossRef](#)]
36. Focacci, F.; D'Antino, T.; Carloni, C. Tensile Testing of FRCM Coupons for Material Characterization: Discussion of Critical Aspects. *J. Compos. Constr.* **2022**, *26*, 04022039. [[CrossRef](#)]
37. *Fédération Internationale du Béton fib Model Code for Concrete Structures 2010*; Wilhelm Ernst & Sohn: Berlin, Germany, 2013.
38. Caggegi, C.; Carozzi, F.G.; De Santis, S.; Fabbrocino, F.; Focacci, F.; Hojdys, L.; Lanoye, E.; Zuccarino, L. Experimental analysis on tensile and bond properties of PBO and aramid fabric reinforced cementitious matrix for strengthening masonry structures. *Compos. Part B Eng.* **2017**, *127*, 175–195. [[CrossRef](#)]
39. Carozzi, F.G.; Poggi, C. Mechanical properties and debonding strength of Fabric Reinforced Cementitious Matrix (FRCM) systems for masonry strengthening. *Compos. Part B Eng.* **2015**, *70*, 215–230. [[CrossRef](#)]